2018

Interface bond performance of steel fibre embedded in magnesium phosphate cementitious composite

Hu Feng
Zhengzhou University, hfeng@uow.edu.au

M Neaz Sheikh
University of Wollongong, msheikh@uow.edu.au

Muhammad N. S Hadi
University of Wollongong, mhadi@uow.edu.au

Lu Feng
Zhengzhou University

Danying Gao
Zhengzhou University

See next page for additional authors

Interface bond performance of steel fibre embedded in magnesium phosphate cementitious composite

Abstract

A series of pullout tests were carried out to characterize the interface bond between steel fibre and magnesium phosphate cement (MPC) based matrix. The effect of the mixture proportions, curing time and end-hook of fibre on the interface bond properties between the steel fibre and the MPC-based matrix was investigated. The mixture proportions investigated include the mole ratio of magnesium oxide to potassium dihydrogen phosphate, mass ratio of sand to cement, mass ratio of water to cement and dosage of silica fume. The effect of different types of cement on the interface bond properties was also investigated.

Publication Details

Feng, H., Sheikh, M. Neaz., Hadi, M. N. S., Feng, L., Gao, D. & Zhao, J. (2018). Interface bond performance of steel fibre embedded in magnesium phosphate cementitious composite. Construction and Building Materials, 185 648-660.

Authors

Hu Feng, M Neaz Sheikh, Muhammad N. S Hadi, Lu Feng, Danying Gao, and Jun Zhao

Interface bond performance of steel fibre embedded in magnesium phosphate cementitious composite

Hu Feng[a] M. Neaz Sheikh[b]* Muhammad N.S. Hadi[b] Lu Feng[a] Danying Gao[a] Jun Zhao[a]

[a]School of Civil Engineering, Zhengzhou University, Henan, 450001, China

[b]School of Civil, Mining and Environmental Engineering, University of Wollongong, NSW 2522, Australia

Correspondence:

M. Neaz Sheikh

School of Civil, Mining & Environmental Engineering

University of Wollongong, Australia

E-mail: msheikh@uow.edu.au

Telephone: + 61 2 4221 3009

Facsimiles: + 61 2 4221 3238

---

* Corresponding author

Interface bond performance of steel fibre embedded in magnesium phosphate cementitious composite

Abstract: A series of pullout tests were carried out to characterize the interface bond between steel fibre and magnesium phosphate cement (MPC) based matrix. The effect of the mixture proportions, curing time and end-hook of fibre on the interface bond properties between the steel fibre and the MPC-based matrix was investigated. The mixture proportions investigated include the mole ratio of magnesium oxide to potassium dihydrogen phosphate, mass ratio of sand to cement, mass ratio of water to cement and dosage of silica fume. The effect of different types of cement on the interface bond properties was also investigated.

Keywords: Pullout; Steel fibre; Magnesium phosphate cement; Physicochemical bond; Mechanical bond.

Highlights

- Interface bond between steel fibre and MPC based matrix was investigated
- Bond properties were influenced significantly by the compressive strength of matrix
- End-hooks of the steel fibre improved significantly the bond properties
- Bond properties improved by the incorporation of silica fume up to 10% by mass
- Effect of different types of cement on the bond properties was also investigated

1. Introduction

Magnesium phosphate cement (MPC) is a new type of binder in which the chemical bond is formed by acid-base reactions between magnesia and phosphate. Compared to the ordinary Portland cement, the MPC possesses many excellent properties including very rapid setting, high early strength, ability to set and harden at temperatures as low as -20° C, low shrinkage, high bond strength, high abrasion resistance and high durability. Therefore, the study and applications of MPC as a repair and quick-construction material have received significant attention in recent years [1-7].

The MPC-based composites have excellent engineering properties; however, they are typically brittle in nature and have inherent weaknesses in resisting tension. Moreover, they are more brittle than the ordinary Portland cement (OPC) and sulphoaluminate cement (SAC) based matrix because of the high volume of cementitious compounds [8]. It has been recognized that the behaviour of such materials can be significantly improved by the addition of discontinuous fibres [9]. The results of some studies indicated that the addition of the proper type and amount of fibres into MPC-based matrix led to composites with an elastic-plastic or deflection hardening behaviour under bending [10]. The steel fibre is one of the most widely used fibres for improving the strength, ductility and toughness of brittle cementitious composites due to the ease of application together with its high efficiency. The chemical bond strength between the steel fibre and the MPC-based matrix was higher than chemical bond strength between the steel fibre and the sulphoaluminate cement (SAC)-based matrix [11, 12]. The addition of steel fibre improved significantly the compressive strength, flexural strength, flexural toughness and flexural ductility of MPC-based composites [13]. The improvement in composite properties is largely attributed to the bond between the steel fibre and the matrix. The steel fibre-matrix interface bond strongly influences the ability of fibres to stabilize crack propagation in the matrix. The interface bond between the steel fibre and the cementitious matrix can be separated into physicochemical and mechanical contribution. The physicochemical bond contribution is predominantly influenced by the cementitious matrix packing density and the properties of the fibre surface (i.e., smooth, etched, or roughened). The mechanical bond contribution is influenced by the

75 geometric deformation of the fibre and the transverse tensile stress resistance of the matrix [14]. The
76 packing density and transverse tensile stress resistance of the matrix are related to the mixture
77 proportions of the matrix and curing time. While some studies provided preliminary results on the
78 bond properties between steel fibre and MPC-based matrix, a large number of variables are yet to be
79 investigated. The interface bond between the steel fibre and the MPC-based matrix has not yet been
80 fully characterized. The test of pullout fibre embedded in the cementitious matrix is generally used to
81 characterize the fibre-matrix interface bond [9]. The known parameters that govern the mechanical
82 properties of fibre reinforced cementitious composites include fibre type, fibre dimensions [15, 16],
83 fibre geometry [17, 18], volume fraction [19], strength of the fibre-matrix interface [20], surface
84 texture of the fibres [21, 22], fibre combination [23, 24] and fibre distribution [25]. The effects of
85 these parameters on the mechanical properties of fibre reinforced cementitious composites can be
86 investigated by the pullout test.
87
88 A series of pullout tests of steel fibres embedded in the MPC-based matrix were carried out in this
89 study. The effect of the mixture proportions, curing time and end-hook of the fibre on the interface
90 bond properties was experimentally investigated. The mixture proportions of the matrix investigated
91 include the mole ratio of magnesium oxide (MgO) to potassium dihydrogen phosphate (KH_2PO_4),
92 mass ratio of sand to cement, mass ratio of water to cement and dosage of silica fume. The fibres
93 investigated include straight and hooked-end steel fibres. The effect of cement types (MPC, SAC and
94 OPC) on the interface bond properties was also explored. The results obtained from this investigation
95 are important for better understanding the role of steel fibres in improving the strength and toughness
96 of MPC-based composites.
97

98 # 2. Experimental program

99 ## 2.1 Materials

100 The Magnesium Phosphate Cement (MPC) was prepared from a mixture of magnesium oxide (MgO),

101 potassium dihydrogen phosphate (KH_2PO_4) and multi-composite retarder. The multi-composite
102 retarder consisted of borax ($Na_2B_4O_7 \cdot 10H_2O$), disodium hydrogen phosphate dodecahydrate
103 ($Na_2HPO_4 \cdot 12H_2O$) and calcium chloride ($CaCl_2$). The MgO was sourced from Zhengyang Casting
104 Material Company of Xinmi, Henan, China [26] in the form of magnesia powder with a specific
105 surface area of 429 m^2/kg. The detailed chemical composition of MgO is provided in Table 1 [26].
106 The industrial-grade potassium dihydrogen phosphate (KH_2PO_4) with a purity of 98%, particle size of
107 180-385 μm and relative density of 2.338 was supplied by Weitong Chemical Co., Ltd of Wujiang,
108 Jiangsu, China [27]. The industrial-grade borax ($Na_2B_4O_7 \cdot 10H_2O$) with a purity of 95% and particle
109 size of 80-220 μm was provided by Banda Technology Co., Ltd. of Liaoning, China [28]. The
110 disodium hydrogen phosphate dodecahydrate ($Na_2HPO_4 \cdot 12H_2O$) with a purity of 99% and calcium
111 chloride ($CaCl_2$) with a purity of 96% were analytic grade chemical provided by Kermel Chemical
112 Reagent Co., Ltd. of Tianjin, China [29]. The silica fume with a purity of 92% and a specific surface
113 area of 200 m^2/kg was sourced from Nangong Ruiteng Alloy Material Co., Ltd of Hebei, China [30].
114 Tap water and natural river sand with fineness modulus of 2.06 were used in this study.
115
116 The fibre-S and fibre-H were used to investigate the effect of the end hook of the steel fibre on
117 interface bond properties in this study. Both the fibre-S and fibre-H have a smooth surface with a
118 round section. The fibre-S (diameter of 0.75 mm and length of 30 mm length) was straight. The fibre-
119 H (diameter of 0.54 mm and length of 35 mm) was hooked at the end. Table 2 summarizes the
120 properties of steel fibre provided from manufacturers [31]. The sulphoaluminate cement (SAC) of
121 Grade P.O 42.5R according to GB20472-2006 [32] and the ordinary Portland cement (OPC) of Grade
122 P.O 42.5 according to GB175-2007 [33] used in this study were obtained from Anda Special Cement
123 Co., Ltd. Group of Yicheng [34] and Mengdian Group Cement Co., Ltd of Henan, China [35],
124 respectively.
125

126 **2.2 Mixture proportions**

127 The proportions of the mixtures are shown in Table 3. As shown in Table 3, the "M" in the Series

names represents the MPC. The "M/P", "S/C", "W/C" and "SF/C" in the series names represent the MgO-KH_2PO_4 mole ratio, sand-cement mass ratio, water-cement mass ratio and percentage of silica fume to cement by mass, respectively. The magnesium phosphate cement consists of the magnesium oxide (MgO) and potassium dihydrogen phosphate (KH_2PO_4). The default values of MgO-KH_2PO_4 mole ratio, sand-cement mass ratio, water-cement mass ratio and silica fume dosage for the MPC-based matrix are 4, 0.8, 0.14 and 0%, respectively. When one of the variables was changed in the experimental program, the other variables were kept fixed. The dosage of multi-composition retarder was 9.0% of MgO by mass for all MPC matrices. The mass ratio of borax ($Na_2B_4O_7{\cdot}10H_2O$), disodium hydrogen phosphate dodecahydrate ($Na_2HPO_4{\cdot}12H_2O$) and calcium chloride ($CaCl_2$) in the multi-composition retarder was 1:3:1.

2.3 Specimen preparation

The solid raw materials, included the cement (magnesium oxide and potassium dihydrogen phosphate), borax and sand were mixed evenly by a mixer at a low speed. Then the water was added into the mixer and mixed at a low speed for 30 s, followed by a high speed mixing for 60 s. The mixture was cast into the steel moulds, and the steel moulds were compacted on a vibration table. The specimens of MPC-based, SAC-based and OPC-based composites were demolded after 1 hour, 3 hours and 12 hours of casting, respectively. Finally, the specimens were cured in a standard curing room with 95% relative humidity and 20° C temperature. The specimens of Series M-M/P-4 were cured for 6 hours, 12 hours, 1 day, 3 days, 7 days and 28 days to investigate the effect of curing time. All the other specimens were cured for 7 days.

The 50 mm × 50 mm × 50 mm prism specimens were used to test the compressive strength according to ASTM C109M-13 [36]. The dog-bone shaped specimens were used to test the pullout behaviour of four embedded steel fibres within the matrix according to JCI SF-8 [37] and CECS 13:2009 [38]. As shown in Figure 1, the dog-bone shaped specimen was divided into two halves (namely the pullout half and fixed half) by a steel partitioning board with a thickness of 1.0 mm in the middle. The two

155 halves of the specimen were bridged by four steel fibres. The partitioning board had four 0.5 mm
156 diameter holes spaced at 8 mm. The casting process of the paste was completed in three steps: casting
157 the pullout half, installing fibres and casting the fixed half. At first, the paste was cast in the pullout
158 half of the steel mould. Secondly, four fibres were inserted into the paste through the four holes of the
159 partitioning board. The four fibres were carefully arranged to keep them perpendicular to the
160 partitioning board. The embedment lengths of fibre-S and fibre-H in the pullout half of specimens are
161 8 mm and 9 mm, respectively. The embedment lengths of fibre-S and fibre-H in the fixed half of
162 specimens are 22 mm and 26 mm, respectively. The fibres were pulled out from the pullout half
163 during the pullout tests because of the much longer embedment length in the fixed half of specimens.
164 After 1 hour, 3 hours and 12 hours of the casting of specimens prepared with MPC, SAC and OPC,
165 respectively, the fibres were fixed by the hardened paste in the pullout half of the steel mould. The
166 mould was disassembled and the partitioning board was removed. Next, the pullout half of specimen
167 was covered with the cling wrap in order to completely prevent adhesion between the two halves of
168 the specimen and put back into the mould, as shown in Figure 2. Finally, the paste was cast into the
169 other half (fixed half) of the steel mould.
170

171 **2.4 Test procedure**

172 The fibre pullout test was conducted by using an electronic universal testing machine with a capacity
173 of 5 kN. The slip between the fibre and matrix was measured by an extensometer clamped onto the
174 specimen, as shown in Figure 3. The pull loading rate was 0.5 mm/min of the slip. All the readings
175 (pullout load and slip) were collected by the electronic universal testing machine. There were five
176 specimens for each series of the fibre pullout tests. In order to compare the effect of variables on bond
177 performance, all displayed experimental results represent the calculated average curve or average
178 value of each series based on the test results of five specimens. The displayed curves of each series
179 were obtained by averaging the pullout load values at regular slip increments. For example, Figure 4
180 shows the pullout-slip curves of the five individual test results and the average of the test results for

Series M-S/C-1.0 with fibre-H. The micro-morphology of the surface of the fibre pulled out from matrix was examined by a Scanning Electron Microscope (SEM JEOL JSM-7500F, Japan).

3 Test results and discussion

3.1 Evaluation parameters of pullout behaviour

Each fibre pullout test is described by the pullout load versus slip (*P*-*s*) behaviour, where P is the pullout load and s is the slip. To simplify the comparison between different series, τ_{av} is defined as the average bond strength based on the maximum pullout load and the initial embedment length [14] and is given by Equation (1).

$$\tau_{av} = \frac{P_{\max}}{\pi \times d_f \times l_p} \quad (1)$$

where, $P_{\max}$ is the maximum of the pullout load; d_f is the diameter of the fibre; l_p is the initial embedment length of the fibre in the pullout half of the specimen.

The total pullout energy, W_P, is the integration of the area under the pullout load-slip curve, and is given by Equation (2).

$$W_P = \int P(s)ds \quad (2)$$

The total pullout energy is usually determined to up to 2.5 mm slip, according to the recommendation in JCI SF-8 [37]. The pullout energy, W_{uv}, is defined as the total pullout energy, W_P, divided by the volume of the embedded portion of the fibre, and is given by Equation (3).

$$W_{uv} = \frac{W_p}{V_{fe}} \quad (3)$$

where, V_{fe} is the volume of the embedded portion of the fibre. The pullout energy, W_{uv}, is used to compare pullout energy of fibre with different diameters.

The higher bond strength can cause a higher tensile and flexural strength of steel fibre reinforced cementitious materials. The pullout energy is the mechanical energy consumed during fibre pullout processing. It is generally agreed that the pullout energy provides the main source of toughness or energy absorption capacity of fibre reinforced cementitious composites [39].

3.2 Effect of ingredients and proportions of mixture on the bond properties

The mixture proportions investigated included MgO-KH_2PO_4 mole ratio (M/P), sand-cement mass ratio (S/C), water-cement mass ratio (W/C) and percent of silica fume to cement by mass (SF). The compressive strength of matrices (f_c'), average bond strength (τ_{av}) and pullout energy (W_{uv}) with various proportions are summarized in Table 4.

(1) The MgO to KH_2PO_3 mole ratio (M/P)

Figure 5 shows the pullout load versus slip behaviour of specimens with varying M/P ranged from 3 to 6 for fibre-S and fibre-H embedded in MPC-base matrix. Figure 6 and Figure 7 show the average bond strength (τ_{av}) and pullout energy (W_{uv}) with varying M/P, respectively. It can be observed that the average bond strength and pullout energy for specimens with the M/P of 4 were the highest. Sufficient amount of MgO is required in the MPC to ensure the full reaction with the phosphate. However, the excess MgO reduced the amount of the phosphate in the cement and caused a significant reduction of hydration products. The compressive strength of the matrix with M/P of 4 was the highest, too. This indicated that the transverse tensile stress resistance of matrix was the highest at M/P of 4. The optimal value of M/P was 4 for the interface bond between the steel fibre and the MPC-base matrix in this experiment.

(2) Sand to cement mass ratio (S/C)

Figure 8 shows the pullout load versus slip behaviour of specimens with varying S/C ranged from 0.6 to 1.0 for fibre-S and fibre-H embedded in MPC-base matrix. Figure 9 and Figure 10 show the average bond strength (τ_{av}) and pullout energy (W_{uv}) with varying S/C, respectively. As shown in

231 Figure 9 and Figure 10, the average bond strength and pullout energy for specimens with S/C of 0.8
232 were the highest. The amount of cement in the specimens with S/C of 0.6 was the largest. The water-
233 cement mass ratio was kept constant. Hence, the amount of water in specimens with S/C of 0.6 was
234 the largest too. The heat of hydration of MPC was high [3]. The excess water in the paste with S/C of
235 0.6 gradually evaporated and the pores were left during the hydration process, which increased the
236 porosity of the interface zone between the steel fibre and the matrix. Hence, all the pullout parameters
237 for specimens with the S/C of 0.6 were lower than that for specimens with S/C of 0.8. However, when
238 the amount of cement gradually decreased with the increase of sand-cement mass ratio, the products
239 of hydration reduced. Thus the fibres in the paste with the S/C of 1.0 were not fully coated with the
240 cementitious materials. This is the reason that the pullout parameters of specimens with S/C of 1.0
241 were lower than the pullout parameters of specimens with S/C of 0.8.
242
243 **(3) Water to cement mass ratio (W/C)**
244 Figure 11 shows the pullout load versus slip behaviour of specimens with varying W/C ranged from
245 0.14 to 0.18 for fibre-S and fibre-H embedded in the MPC-base matrix. Figure 12 and Figure 13 show
246 the average bond strength (τ_{av}) and pullout energy (W_{uv}) with varying W/C, respectively. With the
247 increase of water-cement mass ratio (W/C) from 0.14 to 0.18, the average bond strength for fibre-S
248 and fibre-H decreased by 26.7% and 43.7%, respectively, and the pullout energy decreased by 41.6%
249 and 37.1%, respectively. The water in the pastes was useful for improving the workability of the paste.
250 However, the excess water in the paste gradually evaporated due to the high heat of hydration for
251 MPC, and the pores were left during the hydration process. This resulted in a reduction in the density
252 of the interface zone between the steel fibre and the matrix. Meanwhile, the excess water caused a
253 high porosity of matrix and resulted in a low compressive strength.
254
255 **(4) Dosage of silica fume (SF/C)**
256 Figure 14 shows the pullout load versus slip behaviour of specimens with varying contents of silica fume
257 ranged from 0% to 15% for fibre-S and fibre-H embedded in the MPC-base matrix. The interfacial

258 resistance during pullout has been toughened in different extents with various contents of silica fume.
259 The maximum pullout load and fullness of the curve increased with the increase of the content of
260 silica fume up to 10% by mass. The toughening effect in pullout process was the most significant in
261 the cases with silica fume of 10% by mass. However, when the content of silica fume increased to
262 15%, the interfacial-toughening effect decreased. This indicates that for the interfacial-toughening
263 effect, the optimum content of silica fume was 10% by mass. Figure 15 and Figure 16 show the
264 average bond strength (τ_{av}) and pullout energy (W_{uv}) with varying contents of silica fume,
265 respectively. It can be observed that the average bond strength and pullout energy increased with the
266 increase in the content of silica fume up to 10% by mass. In comparison with the matrix without silica
267 fume, the average bond strength (τ_{av}) with silica fume of 10% by mass for fibre-S and fibre-H
268 increased by 27.1% and 71.1%, respectively. The pullout energy (W_{uv}) with silica fume of 10% for
269 fibre-S and fibre-H increased by 67.9% and 34.2%, respectively. The study of J. L. Helfet indicated a
270 correlation of pullout energy to the toughness of steel fiber reinforced cement-based materials. Also,
271 there is a correlation between the bond strength to the tensile and flexural strength of steel fibre
272 reinforced cementitious materials [39]. Therefore, it can be inferred that the incorporation of silica
273 fume can effectively enhance the toughness, tensile strength and flexural strength of MPC-based
274 composite. However, the increase of compressive strength with silica fume from 0 to 10% by mass
275 was only 7.75%. The enhancement in the average bond strength and pullout energy due to silica fume
276 is much more significant than the enhancement in the compressive strength of matrix. The previous
277 study observed that a great amount of cementitious particles adhered to fibre surface after pullout
278 from matrix with silica fume [20]. Consequently, the cementitious particles contributed to the friction
279 and resistance during the fibre pullout process.
280
281 **(5) Effect of compressive strength of the matrix on bond properties**
282 According to the test results with varying mixture proportions presented above, it can be summarized
283 that the average bond strength (τ_{av}) and pullout energy (W_{uv}) are related to the compressive strength

of matrix. As shown in Figure 17 and Figure 18, the average bond strength (τ_{av}) and pullout energy (W_{uv}) for fibre-S and fibre-H increased with the increase of the compressive strength of matrix. The matrix with high compressive strength may provide the strong resistance to transverse tensile stress during fibres pullout process. The compressive strength of the matrix and properties of the interface bond between the steel fibre and the matrix were improved by the optimization of mixture proportions and the incorporation of silica fume.

(6) Mechanical bond contribution due to fibre end hook deformation

In comparison to the pullout behaviour of the straight fibre (fibre-S), the average bond strength (τ_{av}) and pullout energy (W_{uv}) for the hooked-end fibre (fibre-H) were much higher, as shown in Figure 6, 7, 9, 10, 12, 13, and Figure 15 to 18. The end hook deformation of the steel fibre contributed to a significant increase in the average bond strength (τ_{av}) and pullout energy (W_{uv}). The mechanical bond contribution of the hooked-end fibre in comparison to the straight fibre can be assessed according to the increment of the average bond strength ($\Delta\tau_{av}$) and pullout energy (ΔW_{uv}) due to the end hook deformation. The increment of the average bond strength ($\Delta\tau_{av}$) and pullout energy (ΔW_{uv}) due to the end hook deformation were increased significantly with the increase of the compressive strength of matrix, as shown in Figure 19. The increment of the average bond strength ($\Delta\tau_{av}$) due to the end hook deformation increased by 118.26% with the increase of compressive strength from 26.8 MPa to 40.3 MPa. The corresponding increment of the pullout energy (ΔW_{uv}) increased by 83.66%. The mechanical bond contribution due to end hook deformation increased proportionally with the increase of the compressive strength of matrix.

The pullout resistance of fibre-S (smooth and straight) was predominantly controlled by the physicochemical bond properties between the fibre and the matrix. However, the bending resistance of the end hook of the hooked-end fibre under pullout induces pressure on the matrix, which increases the frictional force and thus increases the pullout resistance [25]. Additionally, the end hook

deformation of steel fibre contributed to the mechanical bond between steel fibre and matrix. Hence, the end-hooks of the steel fibre improved the bond properties significantly. However, this mechanical contribution decreases with an increase in the slip and is effective only until the end hook is straightened fully [25]. The end hook of the fibre was straightened to different extents corresponding to the various compressive strength of matrix, as shown in Figure 20. The end hook pullout from the matrix with the compressive strength of 40.03 MPa was almost fully straightened. However, the hook pullout from the matrix with the compressive strength of 30.25 MPa was not fully straightened. The positive effect of the end hook deformation of the steel fibre on the mechanical bond contribution increased with the increase of the compressive strength of the matrix until a critical point was reached where the end hook was fully straightened.

3.3 Effect of the curing time on the bond properties

The specimens of Series M-M/P-4 cured for 6 hours, 12 hours, 24 hours (1 day), 72 hours (3 days), 168 hours (7 days) and 674 hours (28 days) were tested to investigate the effect of curing time. The compressive strength (f_c') of matrices, average bond strength (τ_{av}) and pullout energy (W_{uv}) with varying curing time are reported in Table 5. The tensile strength of the matrix cured for 6 hours and 12 hours were low; the mechanical bond contribution for hooked-end fibres (fibre-H) due to the end hook deformation was significant. The matrices, cured for 6 hours and 12 hours, fractured along the cross-section perpendicularly to the fibre during the pullout process of fibre-H. Hence, the pullout parameters of Series M-M/P-4 cured for 6 hours and 12 hours for fibre-H were not got.

Figure 21 presents the effect of curing time on the pullout load versus slip. Both the maximum pullout load and fullness of the curve increased significantly with the increase of the curing time from 6 hours to 28 days. Figure 22 and Figure 23 show the average bond strength (τ_{av}) and pullout energy (W_{uv}), respectively, with varying curing time. It can be observed that the average bond strength (τ_{av}) and pullout energy (W_{uv}) increased significantly with the increase of the curing time, especially during the

first 3 days (72 hours). The average bond strength (τ_{av}) of fibre-S and fibre-H cured for 3 days were 84.9% and 83.4% of those cured for 28 days, respectively. The pullout energy (W_{uv}) of fibre-S and fibre-H cured for 3 days were 76.5% and 71.8% of those cured for 28 days, respectively. The compressive strength (f_c') of matrix cured for 3 days was 83.0% of that cured for 28 days. The excellent compressive strength (f_c') of the matrix, average bond strength (τ_{av}) and pullout energy (W_{uv}) at early curing time were guaranteed by the fast hydration of MPC. Hence, the tensile strength, flexural strength and toughness of the steel fibre reinforced MPC-based composite at early curing time were high [13].

3.4 Effect of the types of cement on the bond properties

Three types of cement were compared in this experimental program: the magnesium phosphate cement (Series M-M/P-4), sulphoaluminate cement (Series SAC) and ordinary Portland cement (Series OPC), as shown in Table 3. The compressive strength (f_c') of matrices, average bond strength (τ_{av}) and pullout energy (W_{uv}) with various types of cement are reported in Table 6.

Figure 24 presents the effect of cement types on pullout load versus slip. As shown in Figure 23 (a), for fibre-S, the maximum pullout load for specimens prepared with MPC was the highest, which was followed by the specimens prepared with SAC and OPC. There is only the physicochemical bond contribution including friction and chemical adhesion for the straight and smooth steel fibres. Hence, it indicated that the physicochemical bond between the steel fibre and the matrix prepared with MPC was higher than the physicochemical bond between the steel fibre and the matrices prepared with SAC or OPC. In comparison to the SAC and OPC pastes, the MPC paste was slightly acidic at the early stage of hydration, which led to the iron ions release from the surface of the steel fibre. The released iron ions were captured by the phosphate which produced a compact phosphate film on the surface of the steel fibre [22]. Additionally, Figure 25 shows the micro-morphology of the surface of

362 fibre-S pulled out from matrices prepared with various cement. It can be observed that much more
363 cementitious particles adhered to the surface of the fibre pulled out from the MPC-based matrix in
364 comparison to the fibres pulled out from SAC and OPC-based matrices. During pullout process, the
365 abrasion of the magnesium phosphate cementitious particles and wedge effect caused by these
366 particles squeezed between the surface of the fibre and matrix tunnel led to the excellent bond
367 properties between the steel fibre and the MPC-based matrix.
368
369 Figure 26 and Figure 27 show the average bond strength (τ_{av}) and pullout energy (W_{uv}), respectively,
370 with varying cement types. It can be observed that the average bond strength (τ_{av}) and pullout energy
371 (W_{uv}) for fibre pulled out from the MPC-based matrix is the highest, which was followed by those
372 from SAC-based and OPC-based matrix. It can be inferred that the positive effect of the steel fibre on
373 the tensile strength, flexural strength and toughness of MPC-based composite was the most
374 significant. As shown in Figure 25, the increment of the average bond strength ($\Delta\tau_{av}$) for the
375 specimens prepared with MPC was similar to the increment of the average bond strength ($\Delta\tau_{av}$) for
376 the specimens prepared with SAC and OPC. As shown in Figure 26, the increment of the pullout
377 energy (ΔW_{uv}) for the specimens prepared with MPC was similar to the increment of the pullout
378 energy (ΔW_{uv}) for the specimens prepared with SAC and OPC. The compressive strengths of matrices
379 prepared with MPC, SAC and OPC were similar too, as shown in Table 6. Hence, the mechanical
380 bond contribution of the hooked-end fibre was predominantly influenced by the compressive strength
381 of matrix, rather than the type of the cement.
382
383 # 4. Conclusions

384 The effect of the mixture proportions, curing time and end hook of the steel fibre on bond properties
385 between the steel fibre and the MPC-based matrix was experimental investigated. The difference in
386 the interface bond properties between the steel fibre and the matrices prepared with different cements

(MPC, SAC and OPC) was also investigated. The following conclusions can be drawn based on the experimental results presented in this study:

(1) The interface bond properties between the steel fibre and the MPC-based matrix were improved by the proper mixture proportions and the incorporation of silica fume. The interface bond properties were significantly influenced by the compressive strength of the matrix. With the increase of the compressive strength of matrix and the increase of the content of silica fume up to 10% by mass, the average bond strength and pullout energy increased significantly.

(2) The interface bond properties between the steel fibre and the MPC-based matrix were improved significantly by the end hook deformation of the steel fibre. The improvement due to the end hook deformation increased significantly with the increase of the compressive strength of the matrix until a critical point was reached where the end hook was fully straightened.

(3) The interface bond properties (the average bond strength and pullout energy) between the steel fibre and the MPC-based matrix at early curing time were excellent due to the fast hydration of MPC.

(4) The physicochemical bond between the steel fibre and the matrix prepared with MPC was much better than the physicochemical bond between the steel fibre and the matrices prepared with SAC and OPC. The better physicochemical bond was guaranteed by the compact phosphate film on the surface of the steel fibre and the great amount of magnesium phosphate cementitious particles adhered to the surface of the steel fibre during the fibre pullout. However, the mechanical bond contribution due to end hook deformation of the steel fibre was predominantly influenced by the compressive strength of the matrix, rather than the type of the cement.

Acknowledgments

The first author would like to acknowledge the University of Wollongong, Australia, and the China Scholarship Council for supporting his overseas research scholarship. All the authors acknowledge the University of Wollongong, Australia for providing research foundation. Financial support from National Key R&D Program of China (2016YFE0125600), National Natural Science Foundation of China (Grant No. 51308504), Scientific & Technological Project of Henan Province (152102310068) and Training Program of Young-backbone teachers of Universities in Henan Province China are gratefully acknowledged.

References

[1] Y. Li, B. Chen. Factors that affect the properties of magnesium phosphate cement, Constr. Build. Mater. 47 (2013) 977-983

[2] Q. B. Yang, S. Q. Zhang, X. L. Wu. Deicer-scaling resistance of phosphate cement-based binder for rapid repair of concrete, Cem. Concr. Res. 32 (1) (2002) 165-168

[3] Z. Ding, Z. J. Li. Effect of aggregates and water contents on the properties of magnesium phospho-silicate cement, Cem. Concr. Compos. 27 (1) (2005) 11-18

[4] E. Soudée, J. Péra. Mechanism of setting reaction in magnesia-phosphate cements, Cem. Concr. Res. 30 (2) (2000) 315-321

[5] F. Qiao, C. K. Chau, Z. Li. Property evaluation of magnesium phosphate cement mortar as patch repair material, Constr. Build. Mater. 24 (5) (2010) 695-700

[6] D. A. Hall, R. Stevens, B. El-Jazairi. The effect of retarders on the microstructure and mechanical properties of magnesia-phosphate cement mortar, Cem. Concr. Res. 31 (3) (20014) 55-65.

[7] C. K. Chau, Fei Qiao, Zongjin Li. Microstructure of magnesium potassium phosphate cement, Constr. Build. Mater. 25 (6) (20112) 911-7

[8] A. Ezeldin, P. Balaguru. Toughness behavior of fiber reinforced rapid set materials: A Preliminary Study, ASTM Journal, Cement, Concrete, and Aggregates, 14 (1) (1992) 3-7

[9] M. Jamal Shannag, Rune Brincker, Will Hansen. Pullout behavior of steel fibers from cement-based composites, Cem. Concr. Res. 27 (6) (1997) 925-936

[10] Jean Péra, Jean Ambroise. Fiber-reinforced Magnesia-phosphate Cement Composites for Rapid Repair, Cem. Concr. Compos. 20 (1) (1998) 31-39

[11] P.Frantzis, R.Baggott. Transition points in steel fiber pullout tests from magnesium phosphate and accelerated calcium aluminates binders, Cem. Concr. Compos. 25 (1) (2003) 11-17

[12] P.Frantzis, R.Baggott. Bond between reinforcing steel fibres and magnesium phosphate/calcium aluminate binders, Cem. Concr. Compos. 22 (3) (2000) 187-192

[13] H. Feng, G. Chen, D. Gao, K. Zhao, and C. Zhang. Mechanical Properties of Steel Fiber-Reinforced Magnesium Phosphate Cement Mortar, Advances in Civil Engineering, 2018 (2018), Article ID 3978318, doi:10.1155/2018/3978318.

[14] Kay Wille, Antoine E. Naaman. Pullout Behavior of High-Strength Steel Fibers Embedded in Ultra-High-Performance Concrete, ACI Mater. J. 109 (4) (2012) 479-487

[15] A.E. Naaman, S.P. Shah, Pull-out mechanism in steel fiber-reinforced concrete, ASCE J. Struct. Div. 102 (8) (1976) 1537-1548.

[16] L.R. Betterman, C. Ouyang, S.P. Shah. Fiber-matrix interaction in microfiber reinforced mortar, Adv. Cem. Based Mater. 2 (2) (1995) 53-61.

[17] V. Ramakrishnan, T. Brandshaug, W. V. Coyle, E.K. Schrader. A comparative evaluation of concrete reinforced with straight steel fibers and fibers with deformed ends glued together into

bundles, ACI J. Proc. 77 (3) (1980) 135-143
[18] Nemkumar Banthia, Jean-François Trottier. Concrete reinforced with deformed steel fibers part II: toughness characterization, ACI Mater. J. 92 (2) (1995) 146-154
[19] P. Rossi, N. Harrouche. Mix design and mechanical behaviour of some steel fibre-reinforced concretes used in reinforced concrete structures, Mater. Struct. 23 (4) (1990) 256-266.
[20] Y. W. Chan, S. H. Chu. Effect of silica fume on steel fiber bond characteristics in reactive powder concrete, Cem. Concr. Res. 34 (7) (2004) 1167-1172
[21] V.C. Li, Y. Wang, S. Backer. Effect of inclining angle, bundling and surface treatment on synthetic fibre pull-out from a cement matrix, Composites, 21 (2) (1990) 132-140
[22] A. Peled, H. Guttman, A. Bentur. Treatments of polypropylene fibres to optimize their reinforcing efficiency in cement composites, Cem. Concr. Compos. 14 (4) (1992) 277-285
[23] Y. Ohama, M. Miyara, M. Endo. Properties of steel fiber and polyethylene fiber hybrid reinforced polymer-modified concrete, in: The Twenty-eighth Japan Congress on Materials Research, The Society of Materials Science, Japan, Kyoto, 1985, 151-156
[24] N. Banthia, J. Sheng. Micro-Reinforced Cementitious Materials, MRS Online Proceedings Library, 211 (25) (1990)
[25] P. Stähli, R. Custer, J.M. van Mier. On flow properties, fibre distribution, fibre orientation and flexural behaviour of FRC, Mater. Struct. 41 (1) (2008) 189-196
[26] Zhengyang Casting Material Company. Xinmi, Henan, China. http://www.igreenbuy.com/index.php/shop-info-2728.html/ (Accessed on February 2018) (in Chinese)
[27] Weitong Chemical Co., Ltd of Wujiang, Jiangsu, China. https://wjwthg1818.1688.com/ (Accessed on February 2018) (in Chinese)
[28] Banda Technology Co., Ltd. of Liaoning, China. http://www.lnpdkj.com/ (Accessed on February 2018) (in Chinese)
[29] Kermel Chemical Reagent Co., Ltd. Tianjin, China. http://www.tjkermel.com/ (Accessed on February 2018) (in Chinese)
[30] Nangong Ruiteng Alloy Material Co., Ltd. Lutou, Nangong City, Hebei, China. https://xingtai.1688.com/shop/shop1465318039601. (Accessed on February 2018)
[31] Bekaert China Co., Ltd. Shanghai, China. https://www.bekaert.com.cn/ (Accessed on February 2018) (in Chinese)
[32] CS (Chinese Standard) GB20472-2006, Sulphoaluminate Cement (in Chinese)
[33] CS (Chinese Standard) GB175-2007, Common Portland Cement (in Chinese)
[34] Yicheng Anda Special Cement Co., Ltd. Group. Banqiaodian Town, Yicheng, Hubei, China. http://www.hbadtzsn.com/yewu/36.html/ (Accessed on February 2018) (in Chinese)
[35] Mengdian Group Cement Co., Ltd. Huixian, Henan, China. http://www.hnmdjt.com/ (Accessed on February 2018) (in Chinese)

491 [36] ASTM C109 / C109M-16a, Standard Test Method for Compressive Strength of Hydraulic
492 Cement Mortars (Using 2-in. or [50-mm] Cube Specimens), ASTM International, West
493 Conshohocken, PA, 2016, www.astm.org
494 [37] JCI SF-8, Method of test for bond of fibers, Japan Concrete Institute, 2002.
495 [38] CECS 13:2009, Standard test methods for fiber reinforced concrete, China Association for
496 Engineering Construction Standardization, 2009.
497 [39] J. L. Helfet, B. Harris. Fracture toughness of composites reinforced with discontinuous fibers, J.
498 Mat. Sci. 7 (5) (1972) 494-498
499

List of Tables

List of Figures

539 Figure 24 Effect of the types of cement on the pullout load versus slip: (a) fibre-S and (b) fibre-H

540 Figure 25 Micro-morphology of the surface of fibre-S pulled out from the matrices prepared with
541 different types of cement: (a) MPC, (b) SAC and (c) OPC

542 Figure 26 Effect of the types of cement on the average bond strength

543 Figure 27 Effect of the types of cement on the pullout energy

544

545 Table 1

546 Chemical composition of MgO [26]

Composition	MgO	Fe_2O_3	SiO_2	CaO	Others
Mass fraction of the sample (%)	92.53	0.87	3.1	1.6	1.9

547

548 Table 2

549 Properties of steel fibres [31]

Fibre profile	Fibre type	Length (mm)	Diameter (mm)	Tensile strength (MPa)	Shape and Surface
	Fibre-S	30	0.75	≥1100	Straight/Smooth/Round
	Fibre-H	35	0.54	≥1200	Hooked-end/Smooth/ Round

550

551 Table 3

552 Mixture proportions of matrices

Series	Mole ratio of MgO to KH_2PO_3	Mass ratio of sand to cement	Mass ratio of water to cement	Silica fume	Retarder
M-M/P-3	3	0.8	0.14	0	9.0%
M-M/P-4	4				
M-M/P-5	5				
M-M/P-6	6				
M-S/C-0.6	4	0.6	0.14	0	9.0%
M-S/C-0.8		0.8			
M-S/C-1.0		1.0			
M-W/C-0.14	4	0.8	0.14	0	9.0%
M-W/C-0.16			0.16		
M-W/C-0.18			0.18		
M-SF/C-0	4	0.8	0.14	0	9.0%
M-SF/C-5				5%	
M-SF/C-10				10%	
M-SF/C-15				15%	
SAC	-	2.5	0.36	0	-
OPC	-	1.0	0.50	0	-

553 Note: The MPC consists of magnesium oxide (MgO) and potassium dihydrogen phosphate (KH_2PO_4). The
554 silica fume dosage is the percentage of MPC by mass. The retarder dosage for all the MPC composites is 9.0%
555 of MgO by mass.
556

Table 4

Pullout parameters derived from test results with various proportions

Variables		Type of fibre	Compressive strength of matrix, f_c' (MPa)	Average bond strength, τ_{av} (MPa)	Pullout energy, W_{uv} ($N \cdot mm/\text{mm}^3$)
M/P	3	Fibre-H	24.9	8.18	123.70
	4		37.4	12.02	173.06
	5		37.0	11.31	158.46
	6		30.6	9.49	125.44
	3	Fibre-S	24.9	2.72	24.20
	4		37.4	4.53	53.29
	5		37.0	4.46	41.70
	6		30.6	3.51	37.73
S/C	0.6	Fibre-H	34.9	9.24	142.18
	0.8		37.4	12.02	173.06
	1.0		33.1	5.56	123.59
	0.6	Fibre-S	34.9	4.07	43.37
	0.8		37.4	4.53	53.29
	1.0		33.1	3.14	31.81
W/C	0.14	Fibre-H	37.4	12.02	173.06
	0.16		32.0	8.00	135.53
	0.18		26.8	6.77	108.85
	0.14	Fibre-S	37.4	4.53	53.29
	0.16		32.0	3.50	38.68
	0.18		26.8	3.32	31.14
SF/C	0%	Fibre-H	37.4	12.02	173.06
	5%		38.0	13.04	194.92
	10%		40.3	15.28	232.20
	15%		38.6	13.97	209.85
	0%	Fibre-S	37.4	4.53	53.29
	5%		38.0	5.51	61.23
	10%		40.3	7.75	89.48
	15%		38.6	7.10	75.45

Note: The reported values are the average values for each series. The M/P, S/C, W/C and SF/C represent the $MgO\text{-}KH_2PO_4$ mole ratio, sand-cement mass ratio, water-cement mass ratio and percentage of silica fume to cement by mass, respectively.

563 Table 5

564 Pullout parameters derived from test results with varying curing time

Type of fibre	Curing time	Compressive strength of Matrix, f_c' (MPa)	Average bond strength, τ_{av} (MPa)	Pullout energy, W_{uv} ($N \cdot mm/\text{mm}^3$)
Fibre-H	1 d	31.7	8.81	117.82
	3 d	34.6	10.37	144.44
	7 d	37.4	12.02	173.06
	28 d	41.7	12.43	201.21
Fibre-S	6 h	26.5	2.06	24.09
	12 h	30.3	2.90	30.91
	1 d	31.7	3.37	36.52
	3 d	34.6	4.17	42.83
	7 d	37.4	4.53	53.29
	28 d	41.7	4.91	56.02

565 Note: The reported values are the average values for each series.

566

567 Table 6

568 Pullout parameters derived from test results with various types of cement

Type of fibre	Type of cement	Compressive strength of Matrix, f_c' (MPa)	Average bond strength, τ_{av} (MPa)	Pullout energy, W_{uv} ($N \cdot mm/\text{mm}^3$)
Fibre-H	MPC	37.4	12.02	173.06
	SAC	38.0	9.47	135.85
	OPC	38.3	7.48	116.01
Fibre-S	MPC	37.4	4.53	53.29
	SAC	38.0	3.07	30.08
	OPC	38.3	1.74	21.68

569 Note: The reported values are the average values for each series. The MPC, SAC and OPC represent the
570 magnesium phosphate cement, sulphoaluminate cement and ordinary Portland cement, respectively.
571

572

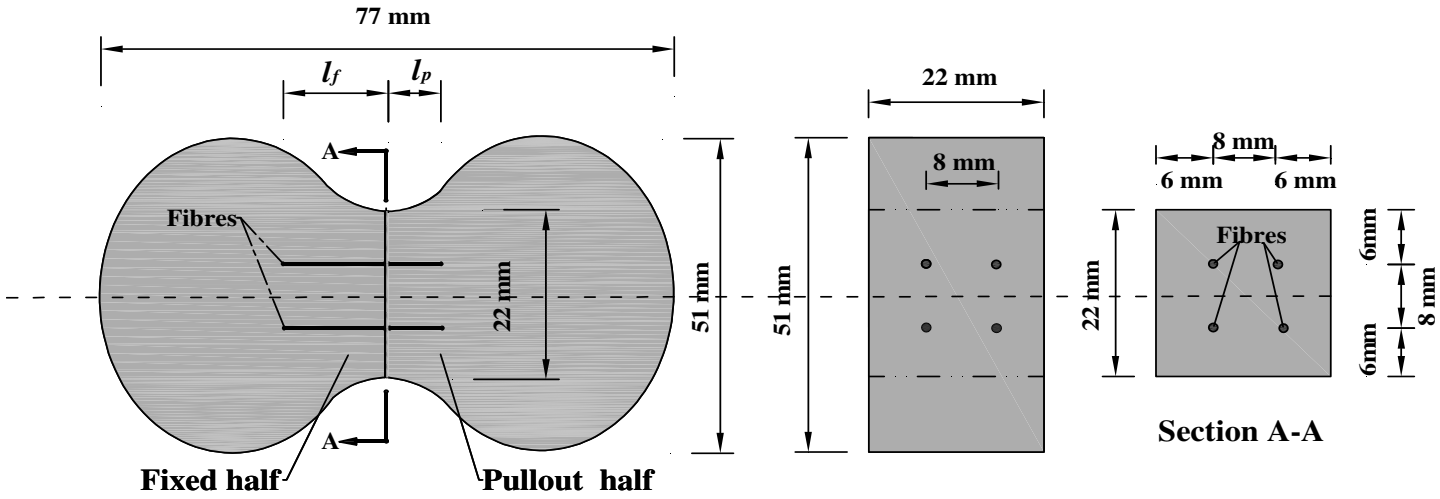

573
574 Figure 1 Illustration of the dog-bone shaped specimen: (a) Top view of the specimen, (b) Side view of the specimen and (c) Section A-A

575 Note: l_f and l_p represent the embedment length of fibre in the fixed half and pullout half of the specimen, respectively.

Figure 2 The fixed half of the specimen covered with a cling wrap in the steel mould

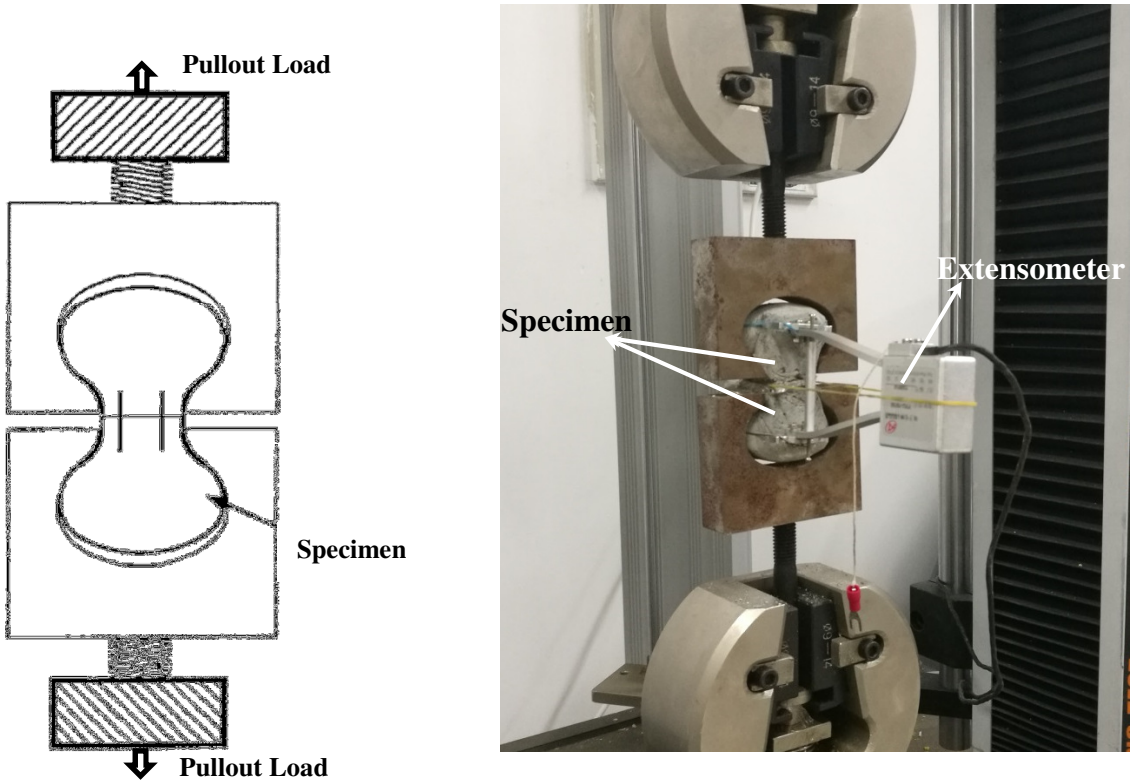

(a) (b)

Figure 3 Pullout test: (a) Schematic representation and (b) Photo of the test

585

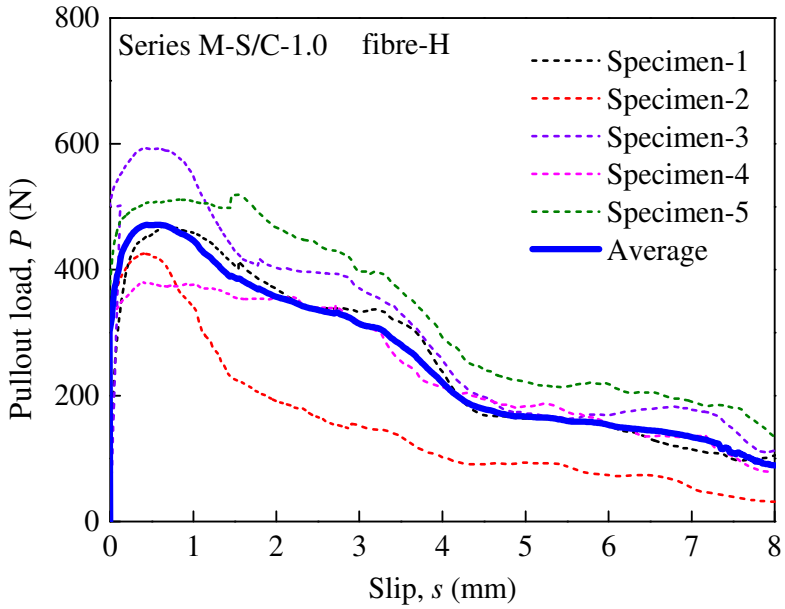

586

587 Figure 4 Pullout-slip curves of Series M-S/C-1.0 together with the averaged plot (fibre-H)

588

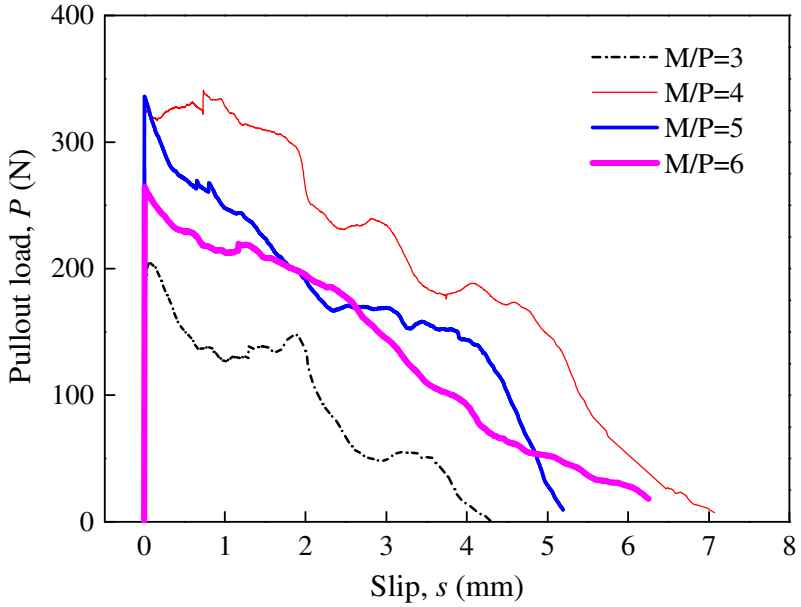

(a)

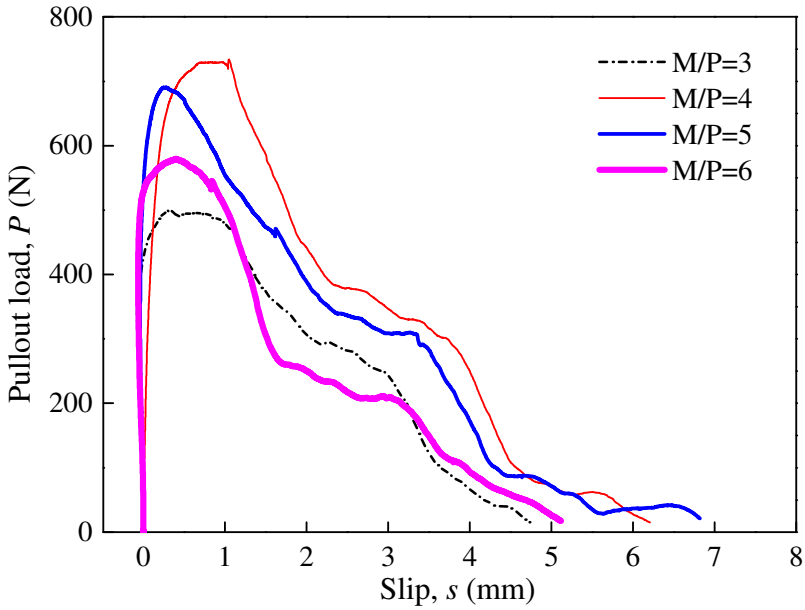

(b)

Figure 5 Effect of M/P on the pullout load versus slip: (a) fibre-S and (b) fibre-H

596

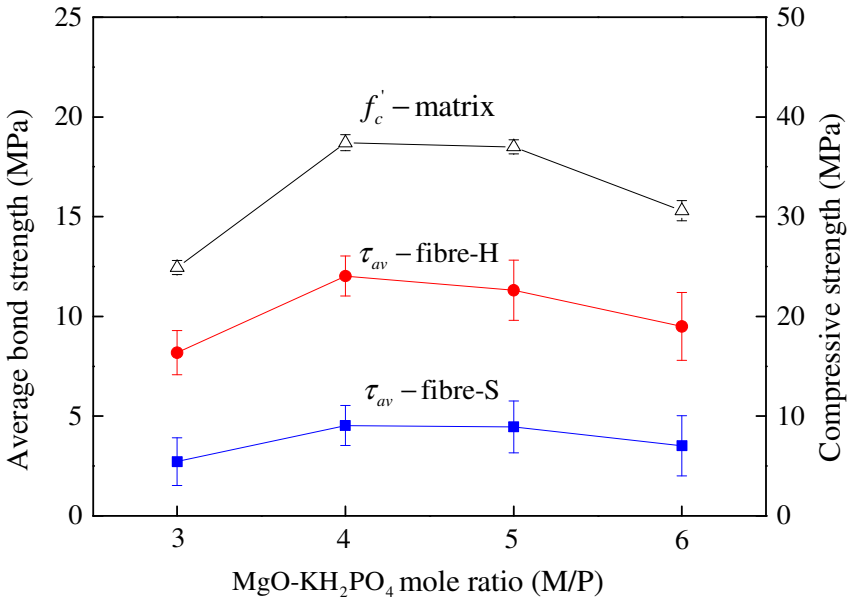

597

598 Figure 6 Effect of M/P on the average bond strength between the steel fibre and the MPC-based
599 matrix (Note: vertical bars represent standard error)

600

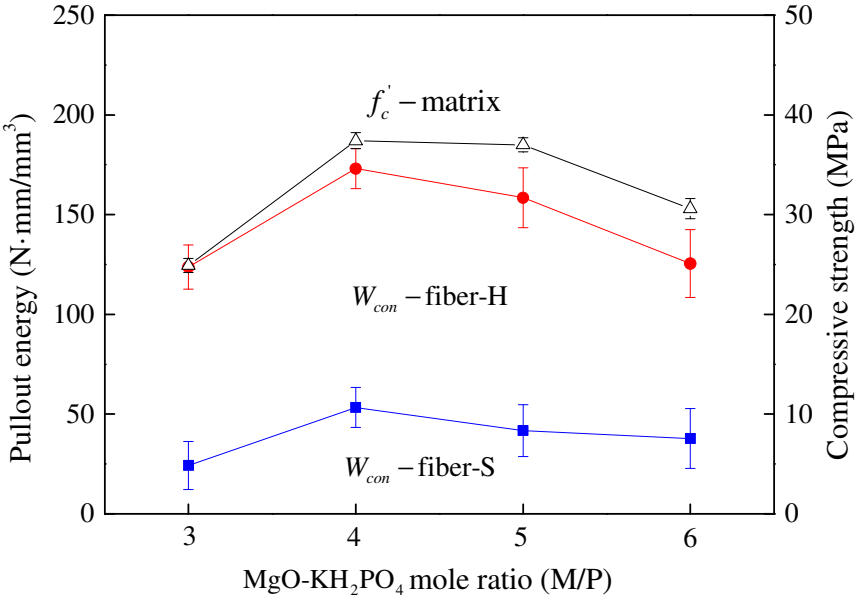

601

602 Figure 7 Effect of M/P on the pullout energy of the steel fibre embedded in the MPC-based matrix
603 (Note: vertical bars represent standard error)

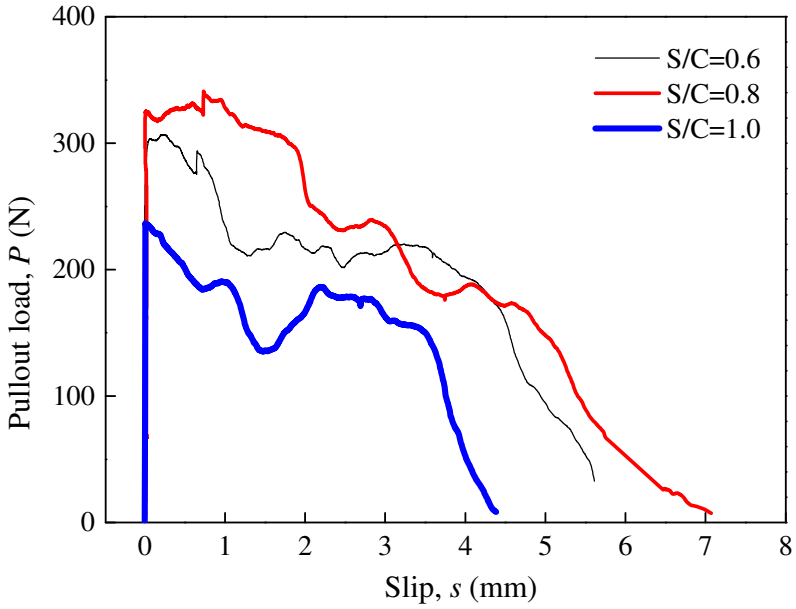

(a)

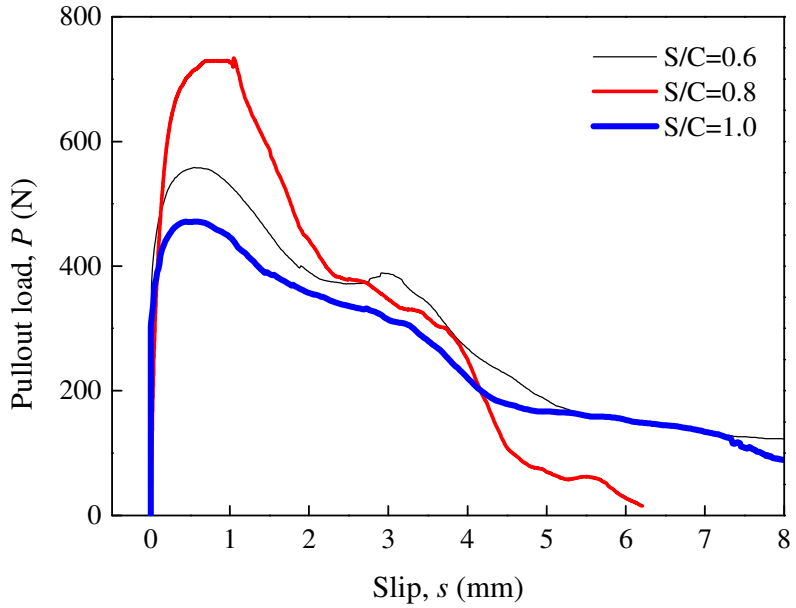

(b)

Figure 8 Effect of S/C on the pullout load versus slip: (a) fibre-S and (b) fibre-H

611

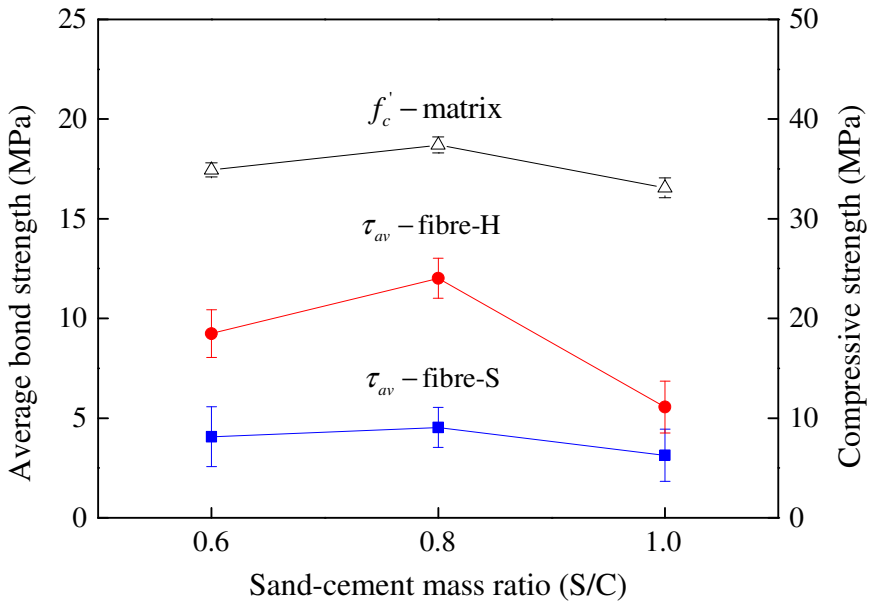

612

613 Figure 9 Effect of S/C on the average bond strength between the steel fibre and the MPC-based matrix

614 (Note: vertical bars represent standard error)

615

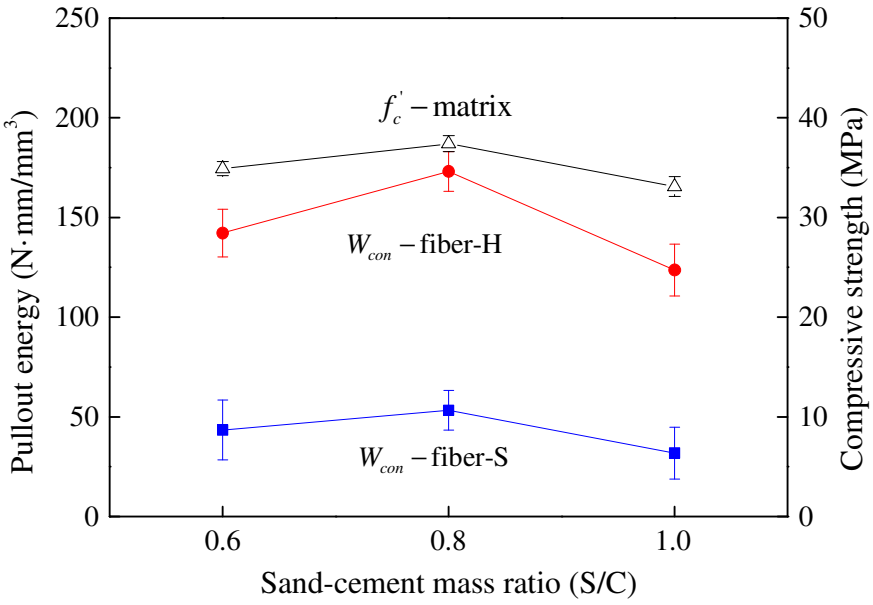

616

617 Figure 10 Effect of S/C on the pullout energy of the steel fibre embedded in the MPC-based matrix

618 (Note: vertical bars represent standard error)

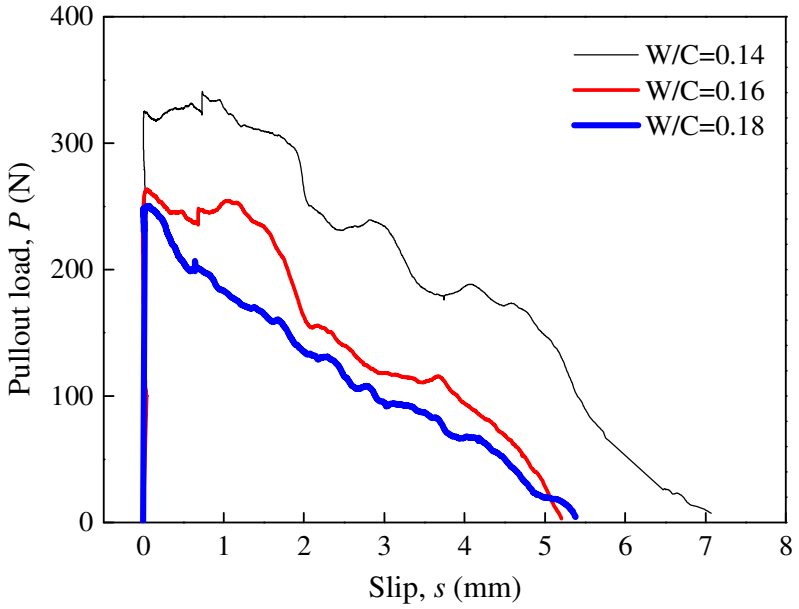

(a)

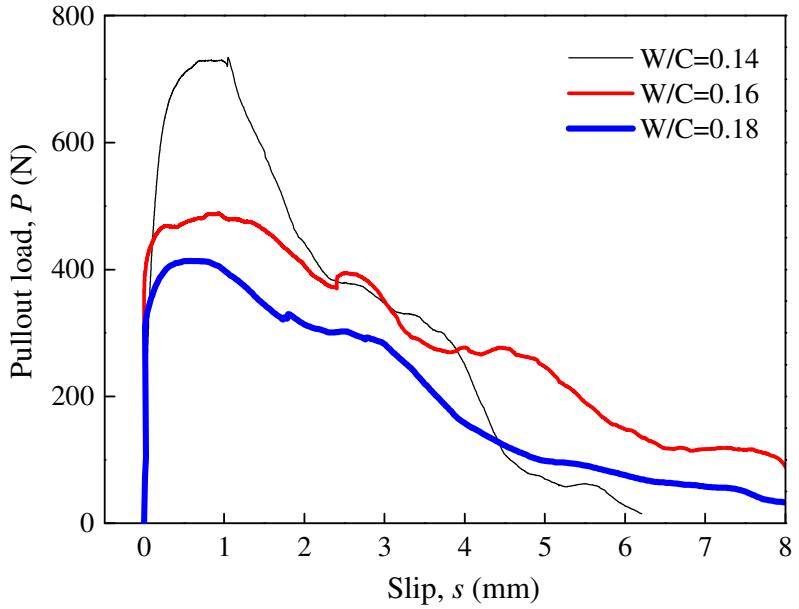

(b)

Figure 11 Effect of W/C on the pullout load versus slip: (a) fibre-S and (b) fibre-H

626

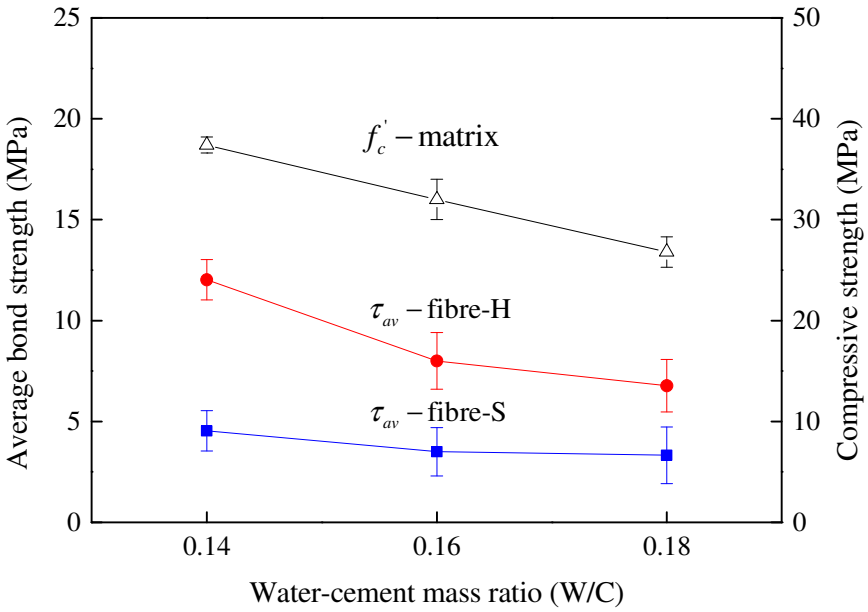

627
628 Figure 12 Effect of W/C on the average bond strength between the steel fibre and the MPC-based
629 matrix (Note: vertical bars represent standard error)

630

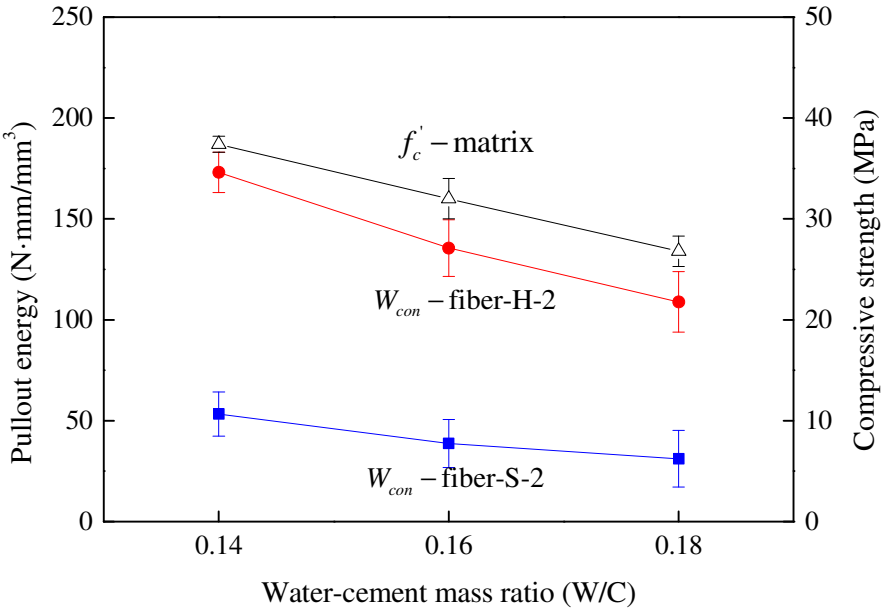

631
632 Figure 13 Effect of W/C on the pullout energy of the steel fibre embedded in the MPC-based matrix

633 (Note: vertical bars represent standard error)

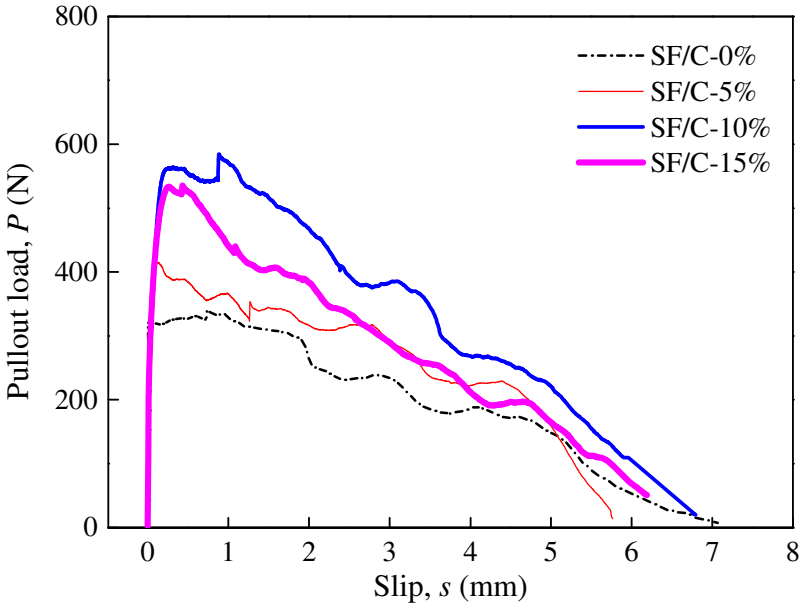

(a)

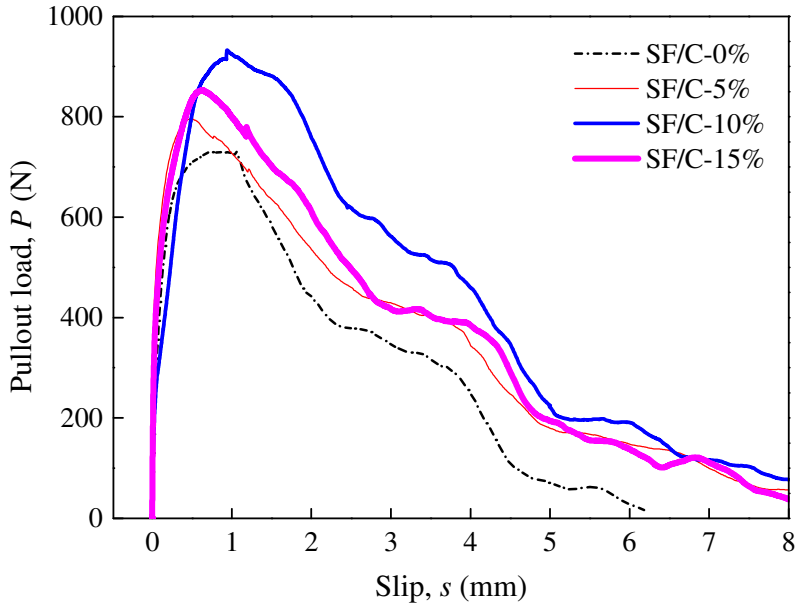

(b)

Figure 14 Effect of the silica fume (SF/C) on the pullout load versus slip: (a) fibre-S and (b) fibre-H

641

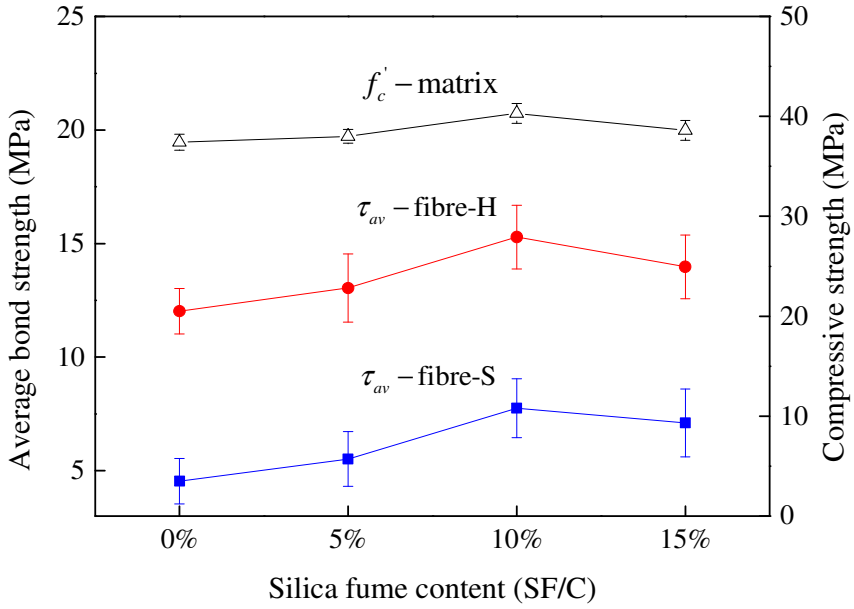

642

643 Figure 15 Effect of the silica fume on the average bond strength between the steel fibre and the MPC-
644 based matrix (Note: vertical bars represent standard error)

645

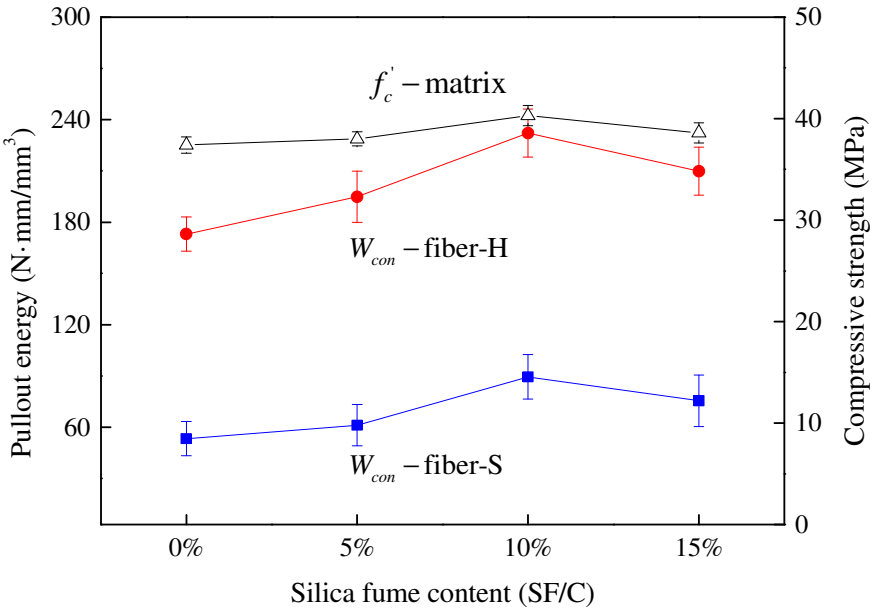

646

647 Figure 16 Effect of the silica fume on the pullout energy of the steel fibre embedded in the MPC-
648 based matrix (Note: vertical bars represent standard error)

649

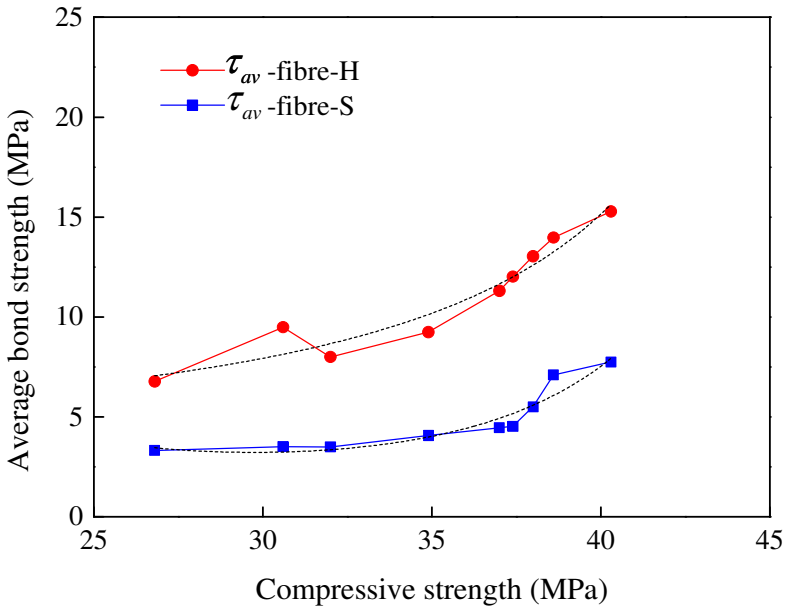

650

651 Figure 17 Effect of the compressive strength of MPC-based matrix on the average bond strength

652

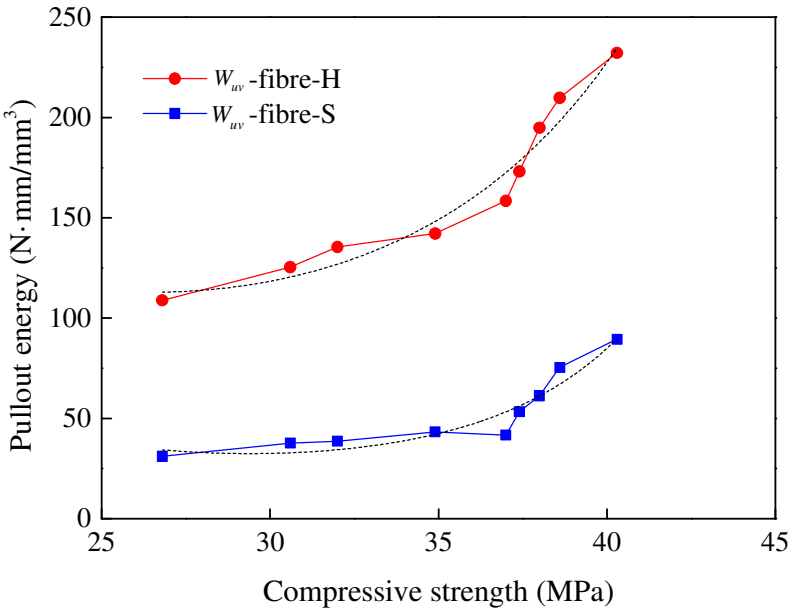

Figure 18 Effect of the compressive strength of MPC-based matrix on the pullout energy

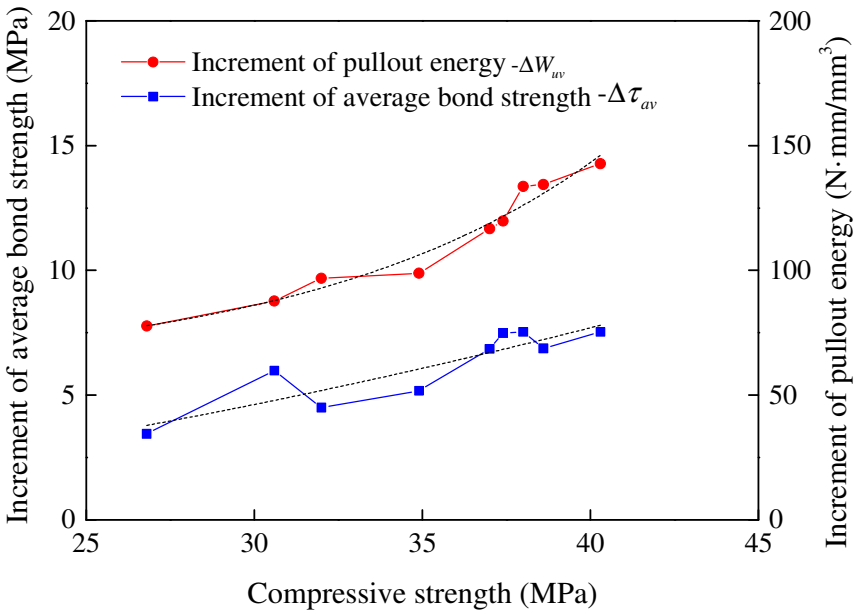

Figure 19 Effect of the end-hook of the steel fibre on the mechanical bond with varying compressive strength of the MPC-based matrix

661

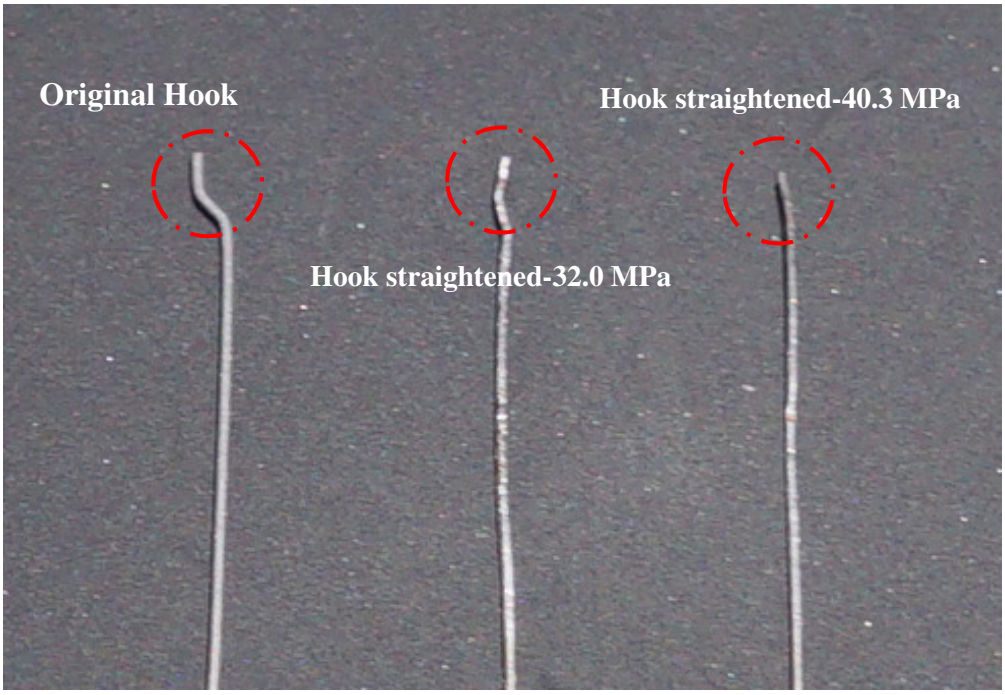

662

663 Figure 20 Hook straightened by the MPC-based matrix with various compressive strengths of matrix

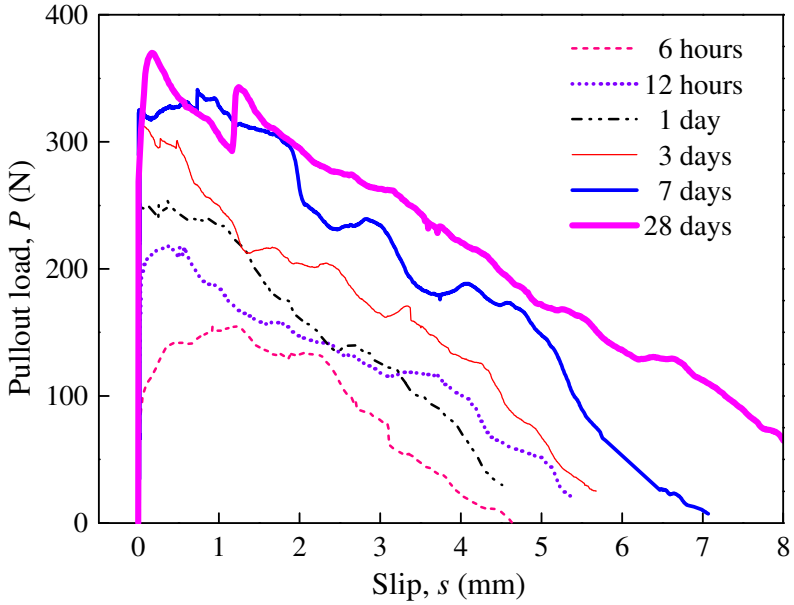

(a)

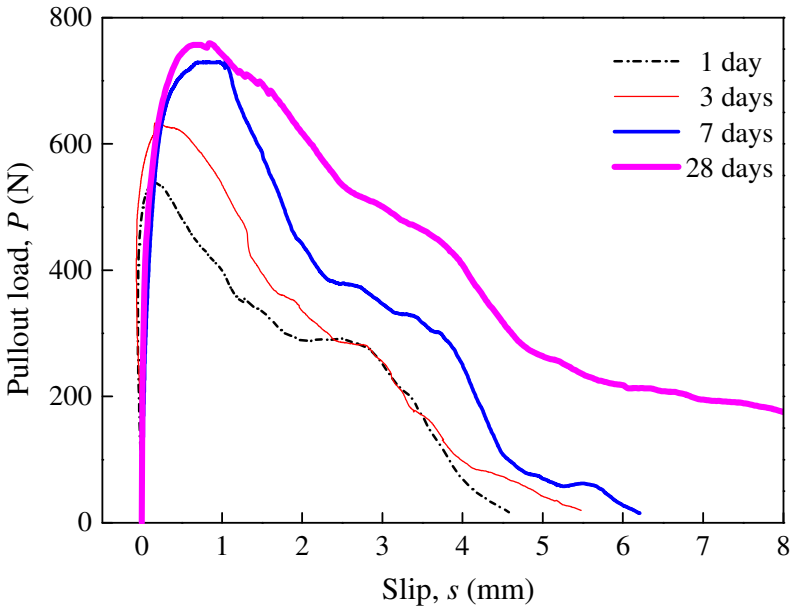

(b)

Figure 21 Effect of curing time on the pullout load versus slip: (a) fibre-S and (b) fibre-H

670

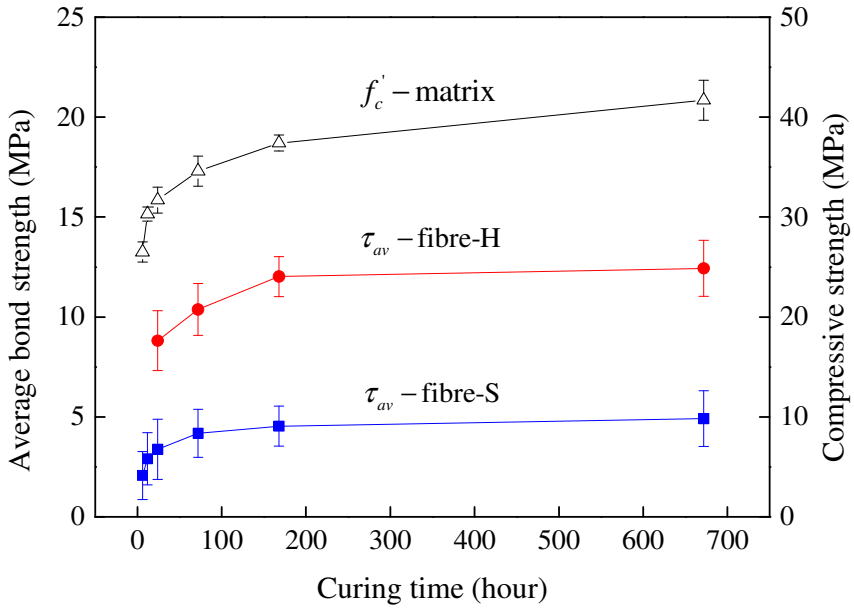

671

672 Figure 22 Effect of curing time on the average bond strength between the steel fibre and the MPC-
673 based matrix (Note: vertical bars represent standard error)

674

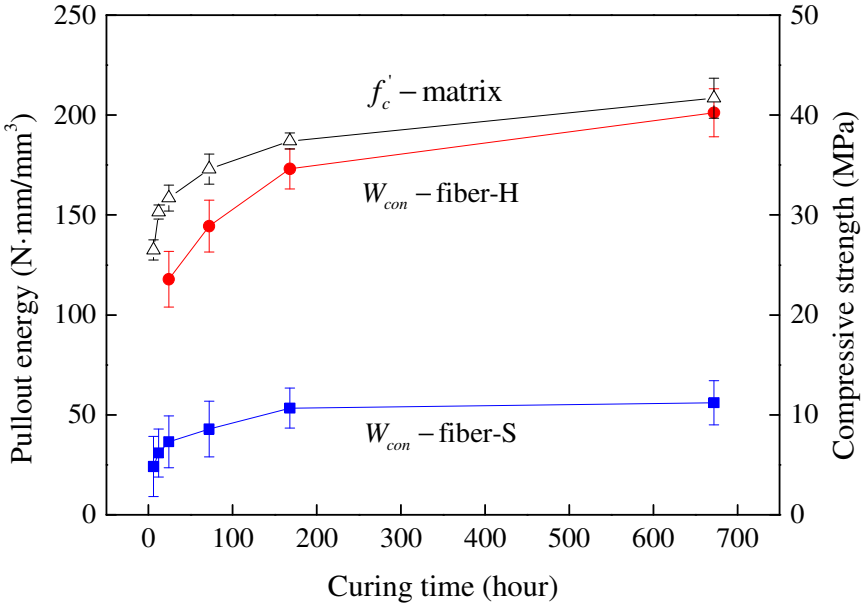

675

676 Figure 23 Effect of curing time on the pullout energy of steel fibre embedded in the MPC-based
677 matrix (Note: vertical bars represent standard error)

678

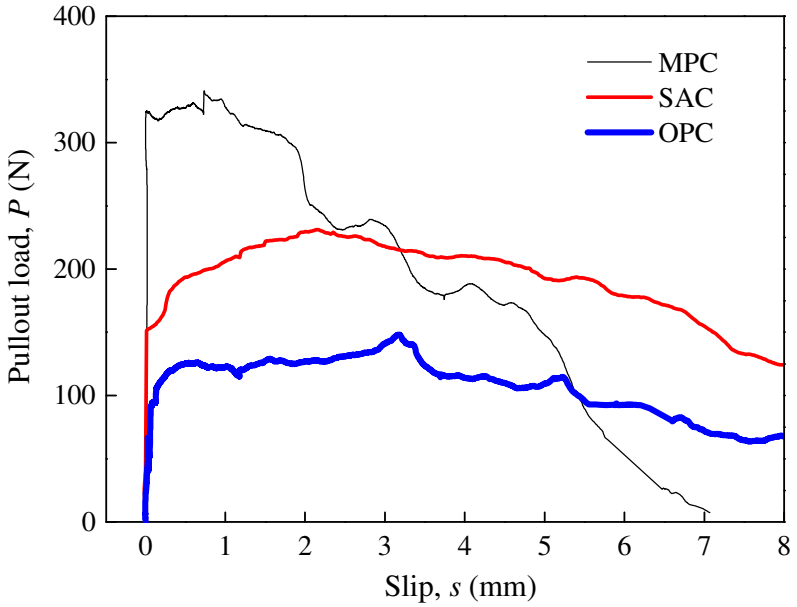

679
680 (a)

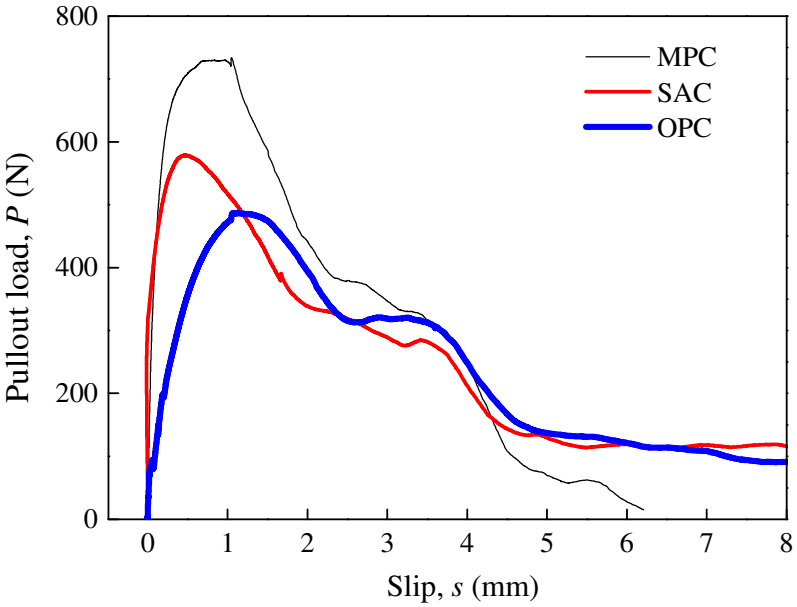

681
682 (b)

683 Figure 24 Effect of the types of cement on the pullout load versus slip: (a) fibre-S and (b) fibre-H

684

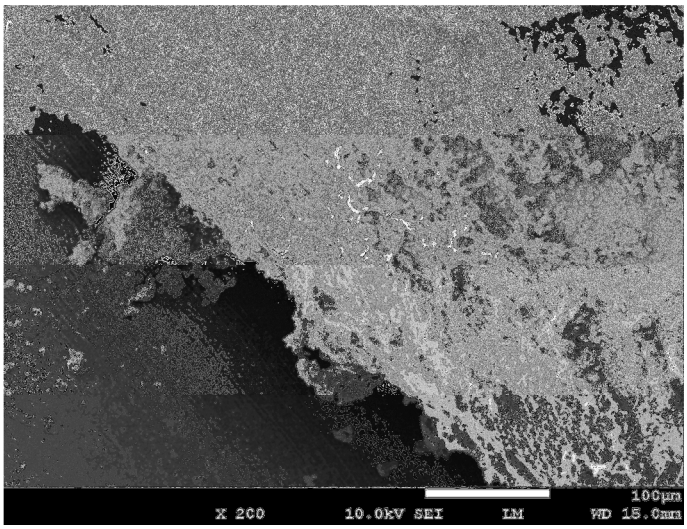

(a)

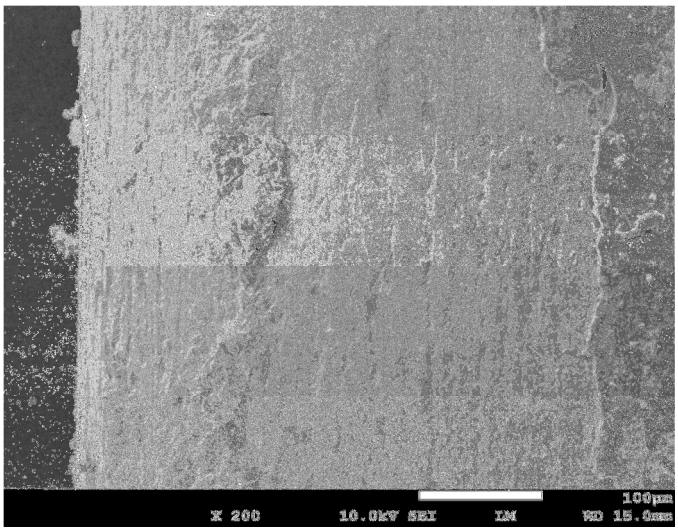

(b)

(c)

Figure 25 Micro-morphology of the surface of fibre-S pulled out from the matrices prepared with different types of cement: (a) MPC, (b) SAC and (c) OPC

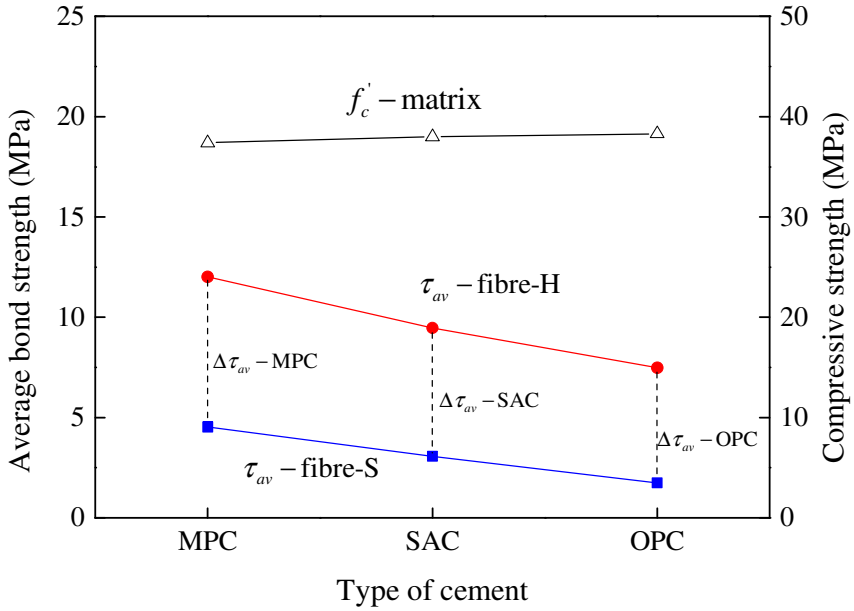

693

694 Figure 26 Effect of the types of cement on the average bond strength

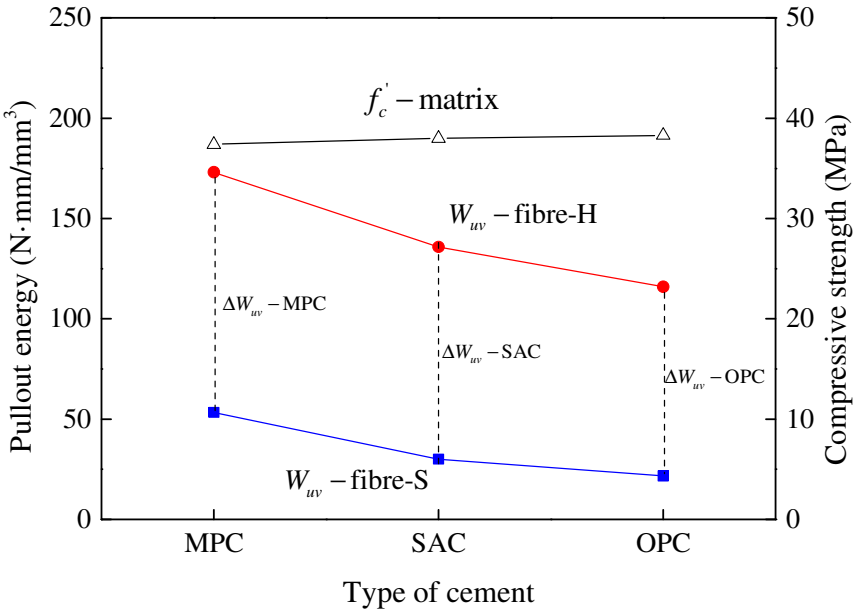

Figure 27 Effect of the types of cement on the pullout energy